Contents lists available at ScienceDirect

Nuclear Engineering and Technology

journal homepage: www.elsevier.com/locate/net

Original Article

Wavelet operator for multiscale modeling of a nuclear reactor

Vineet Vajpayee [a, *], Siddhartha Mukhopadhyay [a, b], Akhilanand Pati Tiwari [a, c]

[a] Homi Bhabha National Institute, Mumbai 400094, India
[b] Seismology Division of Bhabha Atomic Research Centre, Trombay, Mumbai 400085, India
[c] Reactor Control System Design Section of Bhabha Atomic Research Centre, Trombay, Mumbai 400085, India

ARTICLE INFO

ABSTRACT

This article introduces a methodology of designing a wavelet operator suitable for multiscale modeling. The operator matrix transforms states of a multivariable system onto projection space. In addition, it imposes a specific structure on the system matrix in a multiscale environment. To be specific, the article deals with a diagonalizing transform that is useful for decoupled control of a system. It establishes that there exists a definite relationship between the model in the measurement space and that in the projection space. Methodology for deriving the multirate perfect reconstruction filter bank, associated with the wavelet operator, is presented. The efficacy of the proposed technique is demonstrated by modeling the point kinetics nuclear reactor. The outcome of the multiscale modeling approach is compared with that in the single-scale approach to bring out the advantage of the proposed method.

© 2018 Korean Nuclear Society, Published by Elsevier Korea LLC. This is an open access article under the CC BY-NC-ND license (http://creativecommons.org/licenses/by-nc-nd/4.0/).

1. Introduction

A nuclear reactor is a complex time-varying system exhibiting multi-timescale dynamics owing to its large dimensions. This behavior becomes more evident as the system operates through different power regimes. It is well known that modeling using single-scale approach leads to ill-conditioning [1]. Over the years, different approaches have been proposed using two-timescale or three-timescale properties to solve the modeling and control design problem [2—4]. In this work, multiscale property of wavelet basis is used to address the issue.

Some works have been reported for modeling, designing controller, and analyzing dynamic properties of nuclear plants using single-scale approaches such as Auto-Regressive with Exogenous input (ARX), Auto-Regressive Moving Average with Exogenous input, output error (OE), and Subspace methods. For instance, Boroushaki et al. [5] used ARX model for identification of reactor core. Parametric modeling approaches (ARX, Auto-Regressive Moving Average with Exogenous, and OE) require that the model structure of the process be known *a priori*. These techniques may not guarantee global minimum. Furthermore, their complexity

increases with the order of the system to be estimated. On the other hand, subspace methods are robust, computationally efficient, and free from nonconvergence issues. They have been used in nuclear spectroscopy to identify the poles of a system [6] and for the identification of light charged particles [7]. However, multiscale features may not be modeled correctly by the previously discussed techniques. Therefore, it is essential to conduct process visualization and modeling exercise in a multiresolution framework.

Multiscale behavior of a process can be suitably modeled using generalized basis functions in specific wavelet basis functions. The primary advantage of wavelet basis attributes is their ability to estimate a set of low-order linear models of a nonlinear or a multiple timescale system. This is equivalent to breaking down a complex problem into a number of relatively simpler problems, each seen at an appropriate resolution. The idea central to this class of modeling methodology is the invocation of multiresolution analysis (MRA) in data-driven modeling. MRA with wavelet basis functions was first introduced by Mallat in his pioneering work [8]. The last three decades have seen a number of research works dealing with identification of deterministic and stochastic systems from input—output data projected on wavelet basis functions [9—14]. Most existing works in the literature have reported identification of linear time-varying models that attempt to linearly approximate the system output although wavelets are known to provide near-optimal nonlinear estimates of signals. Moreover, all the aforementioned techniques seem to have ignored well-

---

established filter bank theory for output synthesis and have relied more on the linear function approximation approach with wavelet basis, relegating the techniques to off-line identification of the process models. Furthermore, state-space models suitable for designing state feedback control are very rarely found. The limitations of existing techniques justify the need for the development of wavelet operators to transform system states in projection space.

Wavelet-based techniques have found wide application in nuclear engineering for noise removal [15—17], transient detection [18,19], and modeling and control [20—23]. Heo et al. [15] designed a wavelet-PCA—based denoising scheme for the estimation of thermal power. Park et al. [16] demonstrated the application of wavelet denoising in water-level control of steam generators. In the study by Vajpayee et al. [17], the authors applied wavelets to improve the control performance of a predictive controller. Espinosa-Paredes et al. [18] studied transient instability phenomenon of neutronic power oscillation in a boiling water reactor using wavelet transform. Prieto-Guerrero and Espinosa-Paredes [19] applied wavelet ridges technique for estimation of decay ratio and to further evaluate stability parameters using real neutronic measurements. In the study by Antonopoulos-Domis and Tambouratzis [20], a power spectral density—based system identification strategy is designed during a transient via wavelet MRA. Integration of wavelet MRA with correlation function has been proposed for the determination of stability of a reactor [21]. Minimum memory ARX model with wavelet projections has been developed for liquid zone control system [22]. Recently, a subspace-based approach for multiscale modeling of the reactor core is proposed by Vajpayee et al. [23].

State-space modeling of a system is fundamental to designing of Kalman filter, which has several applications in nuclear reactor process estimation [6,7,23,24]. Hong et al. [25] proposed Kalman filtering in a multiresolution framework implemented over data blocks and demonstrated that it outperforms the classical Kalman filtering technique. However, algorithm complexity increases drastically due to simultaneous decomposition and reconstruction steps. Nounou and Nounou [26] developed multiscale Kalman filtering using nonadaptive wavelet transform in which it is shown that the model structure remains unaltered across all scales, provided analysis wavelets for all states are identical. Generally, in a multiscale system, different dynamic modes evolve at various scales of time, and use of the same model at different detail/approximation space would be rather limiting. It would cause derivation of high-order models leading to large approximation error. The proposed technique suggests use of different wavelet basis functions for different modes/states suitably selected to minimize modeling error. In addition, wavelet operators are designed to impose certain specific structure on the system matrix in projection space. The proposed technique diagonalizes the system matrix to decouple system modes completely for application of independent control actions along the Eigen functions [27]. Furthermore, the technique may be used for designing on-line estimation/control because wavelet-based modeling approach identifies a system with a set of multiscale minimum memory models that are amenable to real-time application. Moreover, for on-line applications of multi-timescale processes, it is often more meaningful to work with models at appropriate scales.

The present article formulates a state-space model with wavelet states for a multivariable system. It proves that one can work with a diagonalized state-space model in wavelet subspaces as well. In other words, the methodology works by embedding in a wavelet operator the ability of extracting cross-correlation across variables. Wavelet operators are designed to systematically orchestrate the evolution of a system model across scales. In fact, the proposed method can be seen as an alternative solution

to the problem posed in the study by Chou et al. [9] with a generalization of imparting additional constraints on the synthesis model that qualifies it as a wavelet operator. Although the present formulation is derived in a deterministic setup, it can be readily adopted in a stochastic framework. The methodology of designing a wavelet operator is explained with simulations. Application of the proposed technique for modeling a nuclear reactor from measurements is demonstrated. Furthermore, the derived projection space model is validated with new sets of measurements. Some case studies with different validation datasets show the advantage of proposed approach over classical approach of measurement space modeling.

The rest of the article is organized as follows: Section 2 introduces the notations used in this work and defines local diagonalizing transform. Section 3 establishes relationship between models in measurement space and those in projection space. It further presents the design of multirate perfect reconstruction filter bank. Section 4 shows application of the proposed methodology on a point kinetics model of a nuclear reactor. Section 5 discusses major achievements of the work and indicates future scope.

2. Wavelet operator

2.1. Notations

System input $u(t)$ and output $y(t)$ are defined in Hilbert space L_2 of real-valued square-integrable functions. Discrete measurements $u[k]$ and $y[k]$, respectively, of input and output belong to l_2, the vector space of square-summable sequences. Measurements $u_j^w[k]/u_j^v[k]$ and $y_j^w[k]/y_j^v[k]$ are considered to be projections of $u[k]$ and $y[k]$ on wavelet basis/scaling functions at any resolution 2^{-j}. Wavelet basis functions and scaling functions span the vector space L_2. Sequence $\{V_j\}_{j \in Z}$ of closed subspaces of L_2 is denoted as a multiresolution approximation with difference space W_j satisfying $V_{j+1} \oplus W_{j+1} = V_j$, for all j, $\oplus$ denoting direct sum of the subspaces.

Let us consider a discrete, linear time invariant (LTI), single input single output, multivariate system of order N, given by one-step-ahead state-space model

$$x[k+1] = Ax[k] + Bu[k], \forall k, \tag{1}$$

where $A \in \mathbb{R}^{N \times N}$, $B \in \mathbb{R}^{N \times 1}$, and $x \in \mathbb{R}^N$, respectively, denote system dynamics matrix, input matrix, and state vector. A sequence $x_j^v(x_j^w)$ belongs to $V_j(W_j)$ at any resolution 2^{-j} while $x[k]$ is considered measurable in V_0. Operators projecting onto the respective subspaces $W_j(V_j)$ are also denoted by the same notation $W_j(V_j)$. Let $x_j^v[k]$ be the kth sample of state vector and $x_{ij}^v[k]$ the ith state variable in $x_j^v[k]$.

Let us denote the state-space model in V_j by (A_j^v, B_j^v). The state equation in V_j at resolution 2^{-j} is written as

$$x_j^v[k+1] = A_j^v x_j^v[k] + B_j^v u_j^v[k], \forall k, \tag{2}$$

or in an expanded form as

$$\begin{bmatrix} x_{1j}^v[k+1] \\ x_{2j}^v[k+1] \\ \vdots \\ x_{Nj}^v[k+1] \end{bmatrix} = A_j^v \begin{bmatrix} x_{1j}^v[k] \\ x_{2j}^v[k] \\ \vdots \\ x_{Nj}^v[k] \end{bmatrix} + B_j^v u_j^v[k], \forall k. \tag{3}$$

In this article, we actually deal with operators with truncated support of length equal to number of states, and hence, let us define the $N \times N$ regression matrix at resolution 2^{-j} as

$$X_j[k] = \begin{bmatrix} x_{1j}^v[k] & x_{1j}^v[k-1] & \cdots & x_{1j}^v[k-N+1] \\ x_{2j}^v[k] & x_{2j}^v[k-1] & \cdots & x_{2j}^v[k-N+1] \\ \vdots & \vdots & \ddots & \vdots \\ x_{Nj}^v[k] & x_{Nj}^v[k-1] & \cdots & x_{Nj}^v[k-N+1] \end{bmatrix}, \tag{4}$$

and $1 \times N$ input matrix at resolution 2^{-j} as

$$U_j[k] = \left[u_j^v[k] \vdots u_j^v[k-1] \vdots \cdots \vdots u_j^v[k-N+1] \right], \tag{5}$$

such that the state-space description of a system in terms of regression matrix $X_j[k]$ can be written as

$$X_j[k+1] = A_j^v X_j[k] + B_j^v U_j[k], \forall k, \tag{6}$$

where A_j^v is $N \times N$ matrix and B_j^v is $N \times 1$ column vector. While elements in a row of X_j are considered to have temporal correlation, it is assumed that the elements in a column are correlated spatially. One of the objectives of the transformation is to make this spatial correlation evident by resolving the states of the system on a new set of basis. For this work, it is considered that the change of basis diagonalizes A_j^v i.e., it completely decorrelates spatially. Primary advantage of such a transformation is that the application of control input along the direction of one basis would only affect the state projected on the same basis. Returning to the formulation of the output equation, we can simply write

$$Y_j[k] = C_j^v X_j[k], \tag{7}$$

where $Y_j[k] = [y_j^v[k] \vdots y_j^v[k-1] \vdots \cdots \vdots y_j^v[k-N+1]]$ and C_j^v is a $1 \times N$ row vector.

2.2. Local diagonalizing transform

A local operator matrix is defined as a matrix that locally transforms system states from one resolution to another operating on the finite length regressor. To be more specific, it operates on the regression matrix at any resolution 2^{-j} to give states in the difference space W_{j+1}. Let us now define the separable local diagonalizing transform as

$$x_{j+1}^w[k] = \mathscr{E}\left(W_j^X X_j^T[k]\right), \tag{8}$$

where local operator W_j^X is also defined as an $N \times N$ matrix

$$W_j^X = \begin{bmatrix} w_{11} & w_{12} & \cdots & w_{1N} \\ w_{21} & w_{22} & \cdots & w_{2N} \\ \vdots & \vdots & \ddots & \vdots \\ w_{N1} & w_{N2} & \cdots & w_{NN} \end{bmatrix}. \tag{9}$$

Operator $\mathscr{E}(.)$ extracts the diagonal elements of the operand matrix and arranges them in a column. Note that $x_{j+1}^w[k]$ is a column vector having diagonal elements of $W_j^X X_j^T[k]$, i.e.,

$$x_{j+1}^w[k] = \begin{bmatrix} w_{11}x_{1j}^v[k] + w_{12}x_{1j}^v[k-1] + \cdots w_{1N}x_{1j}^v[k-N+1] \\ w_{21}x_{2j}^v[k] + w_{22}x_{2j}^v[k-1] + \cdots w_{2N}x_{2j}^v[k-N+1] \\ \vdots \\ w_{N1}x_{Nj}^v[k] + w_{N2}x_{Nj}^v[k-1] + \cdots w_{NN}x_{Nj}^v[k-N+1] \end{bmatrix}. \tag{10}$$

The local operator transforms input and output vector as

$$U_{j+1}^w[k] = W_j^X U_j^T[k]; \quad Y_{j+1}^w[k] = \left(W_j^X Y_j^T[k]\right)^T, \tag{11}$$

where U_{j+1}^w is $N \times 1$ column vector and Y_{j+1}^w is $1 \times N$ row vector. Rows of the local operator W_j^X, defined as an $N \times N$ matrix, play the role of wavelet filters. Let us also define the local inverse operator matrix $(W_j^X)^{-1}$ such that $(W_j^X)^{-1} W_j^X = I$. Computation of each state variable by application of local diagonalizing transform requires N multiplications, where N is the order of the system.

It should be clearly understood at the outset that W_j^X is a local operator that operates on the approximation (indicated by superscript v) at resolution 2^{-j} to produce details (indicated by superscript w) at resolution $2^{-(j+1)}$. Therefore, (A_j^v, B_j^v) models the system in V_j, whereas (A_{j+1}^w, B_{j+1}^w) in W_{j+1}. Section 3 establishes a relation between (A_j^v, B_j^v) and (A_{j+1}^w, B_{j+1}^w).

3. State-space model in transform domain

Consider the state-space description given by (6),

$$X_j^T[k+1] = X_j^T[k]\left(A_j^v\right)^T + U_j^T[k]\left(B_j^v\right)^T. \tag{12}$$

Projection onto wavelet space is achieved by first premultiplying by W_j^X and then applying operator $\mathscr{E}(\cdot)$ on both sides of (12), i.e.,

$$\mathscr{E}\left(W_j^X X_j^T[k+1]\right) = \mathscr{E}\left(W_j^X X_j^T[k]\left(A_j^v\right)^T\right) + \mathscr{E}\left(W_j^X U_j^T[k]\left(B_j^v\right)^T\right). \tag{13}$$

The equivalent state equation in W_{j+1} space is given by

$$x_{j+1}^w[k+1] = A_{j+1}^w x_{j+1}^w[k] + B_{j+1}^w U_{j+1}^w[k], \tag{14}$$

with

$$A_{j+1}^w = \left(\left(W_j^X\right)^T\right)^{-1} X_j^{-1}[k] A_j^v X_j[k]\left(W_j^X\right)^T, \tag{15}$$

and B_{j+1}^w is defined as

$$B_{j+1}^w W_j^X U_j^T[k] = \mathscr{E}\left(W_j^X U_j^T[k]\left(B_j^v\right)^T\right). \tag{16}$$

Note that A_{j+1}^w and B_{j+1}^w are defined to be diagonal matrices so that

$$A_{j+1}^w \mathscr{E}\left(W_j^X X_j^T[k]\right) = \mathscr{E}\left(A_{j+1}^w W_j^X X_j^T[k]\right), \tag{17}$$

$$B_{j+1}^w = \mathscr{D}\left(B_j^v\right). \tag{18}$$

Operator $\mathscr{D}(\cdot)$ arranges the elements of a vector operand along the diagonal of a diagonal matrix. Observe that $\mathscr{D}(\cdot)$ would accomplish the reverse operation of $\mathscr{E}(\cdot)$ i.e., it would give back the original matrix only if it is diagonal to start with. By observation, one can state that the sufficient condition that would satisfy (13) is

$$X_j[k+1] = X_j[k]\left(W_j^X\right)^T A_{j+1}^w \left(\left(W_j^X\right)^T\right)^{-1}$$
$$+ \left(\mathscr{D}\left(B_{j+1}^w W_j^X U_j^T[k]\right)\right)^T \left(\left(W_j^X\right)^T\right)^{-1}, \tag{19}$$

subject to the condition that W_j^X is invertible. System parameters in V_j and those in W_{j+1} are then related as

$$A_{j+1}^w = \left(\left(W_j^X\right)^T\right)^{-1} \overline{A_j^v} \left(W_j^X\right)^T, \tag{20}$$

where $\overline{A_j^v} = X_j^{-1}[k] A_j^v X_j[k]$ and $\overline{B_j^v} = B_j^v$. An important implication of Equations (14)–(20) is that one can work with a state-space model having a specific structure in projection space, spanned by local diagonalizing basis, as well. In addition, given a local diagonalizing operator, there exists a definite relationship between the model in measurement space and that in projection space. This formulation is fundamental to the design of a wavelet operator for multiscale modeling. Because A_{j+1}^w is diagonal, to ensure controllability of the transformed system, column vector B_{j+1}^w should not have any zero row.

In practice, $\mathscr{E}(W_j^X X_j^T[k])$ is implemented by appropriately designing analysis multirate filter bank associated with a wavelet operator. The derived relationship between A_j^v and A_{j+1}^w signifies the data-dependent or adaptive nature of the local diagonalizing transform. This is expected because the transform is designed to meet the objectives locally, and hence, the operator is data dependent. However, the basic structure of the operator matrix remains invariant. On the contrary, wavelet transform, in its basic form, is nonadaptive in nature. Later in this article, the factorization of local diagonalizing operator matrix into a nonadaptive and an adaptive matrix is investigated. Furthermore, the design of a nonadaptive operator matrix that qualifies as a wavelet transform operator is also derived.

The output relation in projection space is derived as follows. Taking the transpose of the output, Equation (7) gives

$$Y_j^T[k] = X_j^T[k]\left(C_j^v\right)^T. \tag{21}$$

Premultiplying both sides of (21) by W_j^X gives

$$W_j^X Y_j^T[k] = W_j^X X_j^T[k]\left(C_j^v\right)^T. \tag{22}$$

Using (8) and (11), the previous equation can be written as

$$\left(Y_{j+1}^w[k]\right)^T = \mathscr{D}\left(x_{j+1}^w[k]\right) R^{-1} \left(C_j^v\right)^T, \tag{23}$$

or simply

$$Y_{j+1}^w[k] = C_j^v \left(R^{-1}\right)^T \mathscr{D}\left(x_{j+1}^w[k]\right), \tag{24}$$

where $R = (W_j^X X_j^T)^{-1} \mathscr{D}(\mathscr{E}(W_j^X X_j^T))$ and $C_{j+1}^w = C_j^v(R^{-1})^T$. Let us define $y_{j+1}^w[k] = Y_{j+1}^w[k]Z$, where $Z = [1 \quad 1 \quad \cdots \quad 1]^T$. Now (24) can be written as

$$y_{j+1}^w[k] = C_{j+1}^w x_{j+1}^w[k]. \tag{25}$$

3.1. Design of a nonadaptive wavelet operator matrix

A careful look at (20) reveals that the rows of the matrix $((W_j^X)^T)^{-1}$ are the left eigenvectors of $\overline{A_j^v}$ and diagonal elements of A_{j+1}^w are the corresponding eigenvalues. Let

$$A_{j+1}^w = diag[\alpha_1 \quad \alpha_2 \quad \cdots \quad \alpha_N], \tag{26}$$

where $\alpha_1, \alpha_2, \cdots, \alpha_N$ are nonzero distinct eigenvalues. Any linear transformation $((W_j^X)^T)^{-1}$, satisfying

$$A_{j+1}^w = \left(\left(W_j^X\right)^T\right)^{-1} \overline{A_j^v} \left(W_j^X\right)^T, \tag{27}$$

can in general be given by [28]

$$\left(\left(W_j^X\right)^T\right)^{-1} = \mathscr{W}_j \mathscr{V}_j \Rightarrow \left(W_j^X\right)^T = \mathscr{V}_j^{-1} \mathscr{W}_j^{-1}. \tag{28}$$

One possible choice is $\mathscr{V}_j^{-1} = Q_j = [\overline{B_j^v}, \overline{A_j^v}\overline{B_j^v}, \cdots, \overline{A_j^v}^{N-1}\overline{B_j^v}]$ with $Q_j \tilde{A}_j = \overline{A_j^v} Q_j$ where

$$\tilde{A}_j = \begin{bmatrix} 0 & 0 & \cdots & -a_N \\ 1 & 0 & \cdots & -a_{N-1} \\ 0 & 1 & \cdots & -a_{N-2} \\ \vdots & \vdots & \ddots & \vdots \\ 0 & 0 & \cdots & -a_1 \end{bmatrix}. \tag{29}$$

here, $(a_1, \cdots, a_N)$ are the coefficients of the characteristic polynomial A_j. Matrix Q_j depends on $\overline{A_j^v}(= X_j^{-1}[k] A_j^v X_j[k])$ and needs to be recomputed adaptively at each k. If the system is controllable, then Q_j is of rank N. Moreover, this article does not deal with uncontrollable systems.

With the choice of Q_j given previously, it is elementary to show that the linear transformation $\mathscr{W}_j$ satisfying $A_{j+1}^w \mathscr{W}_j = \mathscr{W}_j \tilde{A}$ is the product of a diagonal matrix ($\mathscr{M}$) and the Vandermonde matrix (refer Appendix A).

$$\mathscr{W}_j = \mathscr{M} \begin{bmatrix} 1 & \alpha_1 & \cdots & \alpha_1^{N-1} \\ 1 & \alpha_2 & \cdots & \alpha_2^{N-1} \\ \vdots & \vdots & \ddots & \vdots \\ 1 & \alpha_N & \cdots & \alpha_N^{N-1} \end{bmatrix}, \tag{30}$$

where $\mathscr{M} = diag[m_1 \quad m_2 \quad \cdots \quad m_N]$, in which $m_1, m_2, \cdots, m_N \in \mathscr{R}$. In specific, matrix $\mathscr{M}$ can be taken as an identity matrix. Matrix $\mathscr{W}_j$ is translation invariant because $\overline{A_j^v}$ is similar to A_j^v and has the same eigenvalues as that of A_j^v. $\mathscr{W}_j$ is of rank N if all the eigenvalues of $\overline{A_j^v}$ are distinct. Because both $\mathscr{V}_j$ and $\mathscr{W}_j$ are of rank N, W_j^X is also of rank N and is invertible.

Any system (A_j^v, B_j^v) if state controllable in measurement space can be transformed into the controllable form $(\tilde{A}_j, \tilde{B}_j)$. Hence, without any loss of generality, one can work with the system described by $(\tilde{A}_j, \tilde{B}_j)$. In such a case, local diagonalizing operator W_j^X is independent of data (translation invariant) and is denoted by $\tilde{W}_j^X$.

$$\left(\left(\tilde{W}_j^X\right)^T\right)^{-1} = \mathscr{W}_j \Rightarrow \tilde{W}_j^X = \left(\mathscr{W}_j^{-1}\right)^T. \tag{31}$$

It may be observed that although translation invariant, $\tilde{W}_j^X$ is not scale invariant as it depends on the eigenvalues at that resolution.

3.2. Design of analysis high-pass filter

In this subsection, an approach to design analysis high-pass filter (HPF) is presented for a general third-order discrete-time system. A third-order system is nontrivial and would bring out salient features of the design methodology. This is a crucial step as the design of analysis HPF further leads to full filter bank implementation. Let $\mathscr{M} = I$, then the operator $\mathscr{W}_j$ for the system is given by

$$\mathscr{W}_j = \mathscr{M} \begin{bmatrix} 1 & \alpha_1 & \alpha_1^2 \\ 1 & \alpha_2 & \alpha_2^2 \\ 1 & \alpha_3 & \alpha_3^2 \end{bmatrix}. \tag{32}$$

From (31) and (32),

$$\tilde{W}_j^X = \frac{1}{\Delta} \begin{bmatrix} \alpha_2\alpha_3(\alpha_3 - \alpha_2) & (\alpha_2^2 - \alpha_3^2) & (\alpha_3 - \alpha_2) \\ \alpha_1\alpha_3(\alpha_1 - \alpha_3) & (\alpha_3^2 - \alpha_1^2) & (\alpha_1 - \alpha_3) \\ \alpha_1\alpha_2(\alpha_2 - \alpha_1) & (\alpha_1^2 - \alpha_2^2) & (\alpha_2 - \alpha_1) \end{bmatrix}, \tag{33}$$

and Δ is determinant of $\mathscr{W}_j$. Note that all columns of $\tilde{W}_j^X$ add up to zero, except for the first column. Hence, all but the first column qualify to be the high-pass analysis filter in a wavelet filter bank. This automatically satisfies the admissibility condition that the Fourier transform of the filter is zero at zero frequency [8]. Values of filter coefficients originating from the first column are suitably augmented to satisfy the admissibility condition.

Every row of $\left(\tilde{W}_j^X\right)^T$ plays the role of half band high-pass analysis filter $g[-k]$ in two-channel perfect reconstruction multirate filter bank i.e.,

$$g_i[-k] = \left(\tilde{W}_j^X\right)^T_{ik}. \tag{34}$$

Other half band filters in the filter bank, i.e., analysis low pass h, synthesis high-pass $\tilde{g}$, and synthesis low pass $\tilde{h}$ filters, can be designed by satisfying biorthogonality condition thereby giving the full filter bank structure. This is explained in Section 3.3 and further derived in Appendix B.

3.3. Design of two-channel biorthogonal filter bank

The approximation spaces $\{V_j\}_{j \in Z}$ and difference spaces $\{W_j\}_{j \in Z}$ are spanned by integer translates of scaling and wavelet basis functions, respectively. The basic dilation equation defines synthesis scaling function $\tilde{\phi}$ and synthesis wavelet function $\tilde{\psi}$ through two-scale difference equation

$$\frac{1}{\sqrt{2}}\tilde{\phi}\left(\frac{t}{2}\right) = \sum_{k=-\infty}^{+\infty} \tilde{h}[k]\tilde{\phi}(t - k), \tag{35}$$

$$\frac{1}{\sqrt{2}}\tilde{\psi}\left(\frac{t}{2}\right) = \sum_{k=-\infty}^{+\infty} \tilde{g}[k]\tilde{\phi}(t - k). \tag{36}$$

Analysis scaling function $\phi(\cdot)$ and analysis wavelet function $\psi(\cdot)$ are related to $h[k]$ and $g[k]$, respectively, through similar relations. Projections onto $\{V_j\}_{j \in Z}$ and $\{W_j\}_{j \in Z}$ are implemented using the analysis filter bank. Analysis and synthesis filters need to satisfy biorthogonality and perfect reconstruction conditions. The synthesis filter design takes care of alias cancellation thereby resulting in perfect reconstruction. These conditions are summarized in the following.

1) Biorthogonality condition, i.e.,

$$\langle \tilde{h}[k], h[k - 2l] \rangle = \delta[l],$$

$$\langle \tilde{g}[k], g[k - 2l] \rangle = \delta[l],$$

$$\langle \tilde{h}[k], g[k - 2l] \rangle = \langle \tilde{g}[k], h[k - 2l] \rangle = 0.$$

2) Perfect reconstruction condition

$$g[k] = (-1)^{(1-k)}\tilde{h}[1 - k],$$

$$\tilde{g}[k] = (-1)^{(1-k)}h[1 - k].$$

It may be noted here that perfect reconstruction condition essentially leads to biorthogonality condition. For a decimated wavelet transform, wavelet coefficients or wavelet states in next lower resolution are obtained by downsampling of analysis and synthesis filters' outputs by two. Furthermore, filter banks can be designed to have desired number of vanishing moments with compact support. A wavelet function $\psi(t)$ is said to have K vanishing moment if the associated scaling function can generate polynomials up to degree $K-1$. This condition is given as

$$\int_{-\infty}^{+\infty} t^m\psi(t)dt = 0, m = 0, 1, \cdots, K - 1. \tag{37}$$

When designing the filter bank, the vanishing moment constraint is used in addition to the biorthogonality and perfect reconstruction conditions. An analytical example of perfect reconstruction biorthogonal wavelet filter bank (PRBWFB) design is given in Appendix B.

3.4. Proposed algorithm

The proposed methodology of multiscale system modeling uses translation invariant but scale adaptive basis functions that completely decorrelate system states in transform domain. Design of this class of wavelet filter bank is based on the nominal model of the system identified in approximation space. Fig. 1 provides a block diagram of the proposed technique. Steps to obtain a multiscale model are listed below.

1) Identify a low-order LTI model $(\widehat{A}_j^v, \widehat{B}_j^v, \widehat{C}_j^v)$ in approximation space V_j. One can use numerically stable subspace methods to estimate dynamic linear state-space model in deterministic/stochastic setup [6,7,29].
2) Compute transformation $\overline{A}_j^v = X_j^{-1}[k]A_j^vX_j[k]$.
3) Compute eigenvalues and coefficients of PRBWFB at resolution 2^{-j}.
4) Operate on states of the transformed system $(\overline{A}_j^v, \overline{B}_j^v)$ in V_j to obtain states of (A_{j+1}^v, B_{j+1}^v) in V_{j+1} and that of (A_{j+1}^w, B_{j+1}^w) in W_{j+1}.
5) Estimate $(\widehat{A}_{j+1}^w, \widehat{B}_{j+1}^w, \widehat{C}_{j+1}^w)$. The nominal model may be obtained by (15) and (18).
6) Repeat steps 1−5 until $j + 1 = J$, where 2^{-J} is minimum resolution [8, 23].
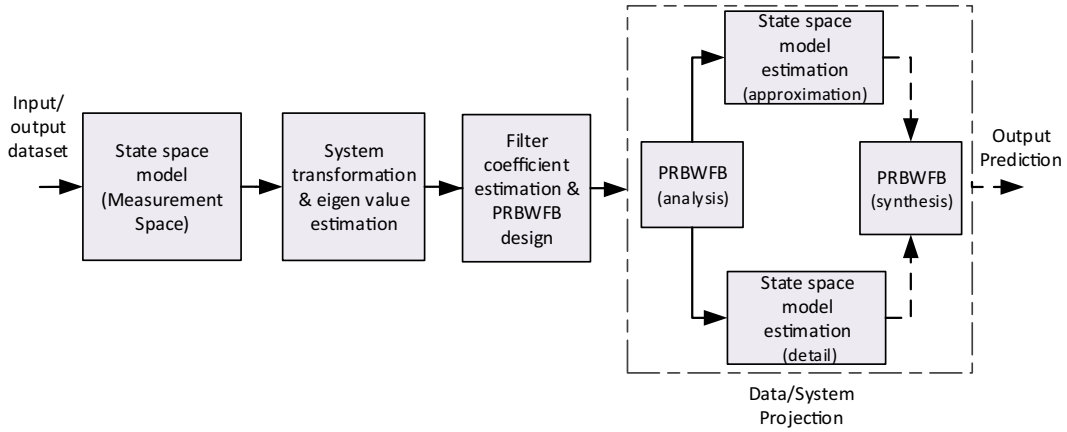
Fig. 1. Block diagram of the proposed projection space modeling technique. PRBWFB, perfect reconstruction biorthogonal wavelet filter bank.

At the end, the multiscale model would consist of a set of LTI models in approximation space V_J and in wavelet spaces W_j, $j = 1, 2, \cdots, J$.

4. Application to nuclear reactor

A nuclear reactor is a complex, nonlinear, multiscale process in which different dynamic modes occur at different time scales. These modes are actually present in the form of clusters, and a reactor is predominantly a two-timescale system [4]. A cluster of modes lying near the origin on the s-plane governs the slow dynamics of the process, whereas the second cluster lying away from the origin is responsible for the fast dynamics. The transient behavior of a nuclear reactor is described by point kinetics model which is a system of nonlinear coupled differential equations. These equations relate the time evolution of reactor power and concentration of delayed neutron precursors with reactivity. The point kinetics model is given by

$$\frac{dP(t)}{dt} = \left(\frac{\rho(t) - \beta}{\Lambda}\right)P(t) + \sum_{i=1}^{6} \lambda_i C_i(t), \tag{38}$$

$$\frac{dC_i(t)}{dt} = \frac{\beta_i}{\Lambda}P(t) - \lambda_i C_i(t), \quad i = 1, 2, \cdots, 6 \tag{39}$$

where ρ is reactivity; P is reactor power; Λ is prompt neutron life time; and λ_i, C_i, and β_i are decay constant, concentration of delayed neutron precursors', and fraction of delayed neutrons of ith group, respectively. The delayed neutron parameters for Uranium-235 are given in Table 1. The steady-state value of power P_0 is set to unity, and Λ is 0.001.

In the following subsections, simulations were performed for two different cases: 1) using reference dataset and 2) using plant dataset. In Section 4.1, an estimation/validation dataset is generated by exciting the point kinetics model with reactivity variation as an input and the corresponding power variation thus obtained as the output of the system. On the other hand, in Section 4.2, plant

Table 1
Delayed neutron parameters for U-235.

Group, i	1	2	3	4	5	6
$\lambda_i(s^{-1})$	0.0124	0.0305	0.1114	0.3013	1.1286	3.013
β_i	0.000215	0.001424	0.001274	0.002568	0.000748	0.000273

datasets obtained from a 540 MWe Indian pressurized heavy water reactor are used for estimation/validation exercise.

4.1. Case study using reference dataset

To develop a wavelet operator for analysis and synthesis and to further model the reactor in projection space, the system given by Equations (38) and (39) needs to be represented in standard state-space form as

$$\dot{x}(t) = Fx(t) + Gu(t), \tag{40}$$

where the state vector x, matrix F, and vector G are defined as

$$x = \begin{bmatrix} P & C_1 & C_2 & C_3 & C_4 & C_5 & C_6 \end{bmatrix}^T, \tag{41}$$

$$F = \begin{bmatrix} -\beta/\Lambda & \lambda_1 & \lambda_2 & \lambda_3 & \lambda_4 & \lambda_5 & \lambda_6 \\ \beta_1/\Lambda & -\lambda_1 & 0 & 0 & 0 & 0 & 0 \\ \beta_2/\Lambda & 0 & -\lambda_2 & 0 & 0 & 0 & 0 \\ \beta_3/\Lambda & 0 & 0 & -\lambda_3 & 0 & 0 & 0 \\ \beta_4/\Lambda & 0 & 0 & 0 & -\lambda_4 & 0 & 0 \\ \beta_5/\Lambda & 0 & 0 & 0 & 0 & -\lambda_5 & 0 \\ \beta_6/\Lambda & 0 & 0 & 0 & 0 & 0 & -\lambda_6 \end{bmatrix}; G = \begin{bmatrix} \frac{\rho P_0}{\Lambda} \\ 0 \\ 0 \\ 0 \\ 0 \\ 0 \\ 0 \end{bmatrix}. \tag{42}$$

Substituting the values of parameters given in Table 1, the open-loop poles of the reactor system described by (40) are observed to be located at

$$s = [0, -0.0143, -0.0678, -0.1929, -0.9970, -2.8318, -6.9953]. \tag{43}$$

Equations (40)–(42) however are the continuous time model. The discrete-time system representation is given by (1) with

$$A = e^{FT_s}, B = \int_0^{T_s} e^{Ft}G dt, \tag{44}$$

where T_s is the sampling period for discretization. The z-domain counterpart of the s-domain poles, for a sampling period of 80 ms, is given by
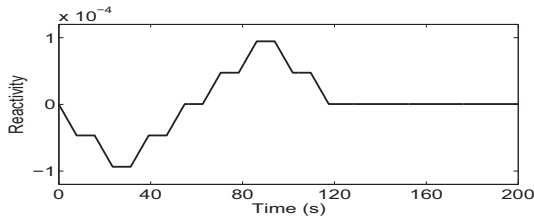
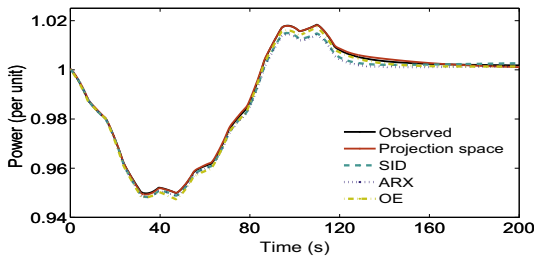**Fig. 2.** Variation of reference reactivity estimation input.

Fig. 3. Outputs of estimated models with observed data for reference input. ARX, Auto-Regressive with Exogenous input; OE, output error; SID, Subspace Identification.

$$z = [0.5714, 0.7973, 0.9233, 0.9847, 0.9946, 0.9989, 1]. \quad (45)$$

To find a relation between input, output, and state variables, the system is excited with a known input signal. One of the ways to change input reactivity to the reactor system is by movement of control rod (CR). It may be noted that insertion of CR from its nominal position introduces negative reactivity which decreases reactor power, whereas withdrawal of CR from its nominal position introduces positive reactivity which increases reactor power. The input reactivity transient is supplied to the point kinetics model of the nuclear reactor to generate variation in the reactor power output. Fig. 2 shows the change in reactivity test input introduced by CR rod movement, and the corresponding reactor power is shown in Fig. 3.

Wavelet operators $\bar{W}_j^X$ are designed using (31) as described in Subsections 3.2 and 3.3. Observe that columns of $\bar{W}_j^X$ play the role of analysis HPF with zero DC gain. These HPFs are used to design synthesis low-pass filters (LPF) by using perfect reconstruction condition. The biorthogonality condition is used to obtain analysis LPF and synthesis HPF. In general, the HPF coefficients obtained by (34) are not symmetric and may cause system of simultaneous equations to be underdetermined. To complete the design of PRBWFB, it is required to have one more design equation. While selecting wavelets for function approximation and to have a sparse representation, the choice is made based on the regularity of the basis function that decides number of vanishing moments and support size. The vanishing moment condition is included as an additional design constraint. The PRBWFBs are designed to have length of eight taps and two vanishing moment as given in Table 2. Measurement space system states are transformed by these operators to those in the projection space, and model parameters are estimated. System dynamics matrix of estimated projection space model is given by A_{j+1}^w

$$A_{j+1}^w = diag[0.6031, \quad 0.7840, \quad 0.9257, \quad 0.9843, \quad 0.9947,$$
$$0.9989, 1]. \quad (46)$$

Different conventional empirical modeling approaches, e.g., SID, ARX, and OE, have also been implemented. The model parameters are estimated from training dataset (Figs. 2 and 3) by minimizing Akaike's Information Criterion. The estimated model parameters are derived in Appendix C. Fig. 3 compares the estimates of the neutron power output obtained by various models with the observed data. It can be observed that all of the models are able to estimate neutron power well enough. However, multiscale features might not have been suitably modeled by any of the single-scale models. A projection space model is expected to sufficiently capture the multiscale process dynamics due to modeling at appropriate scale. Moreover, the fact that the underlying process is nonlinear in nature while all of the estimated models are linear adds to the error in the output.

For the purpose of model validation, two validation datasets have been selected whose dynamics are different from that of the estimation dataset. Furthermore, to demonstrate the efficacy of the proposed techniques, a quantitative comparison with the existing technique has been presented. Validation test inputs shown in Figs. 4 and 6 represent ramp and trapezoidal variations in the reactivity introduced by the movement of CR inside the reactor. They are applied to different estimated models. Outputs of all models are compared with the reference output in Figs. 5 and 7. It is evident that the projection space model shows a better response than the other models.

The modeling performance is quantitatively assessed by computing the percentage mean squared error (PMSE). PMSE between simulation and output observation is calculated by

$$PMSE(\%) = \left(\frac{1}{N} \sum_{k=0}^{N-1} \left(P[k] - \widehat{P}[k] \right)^2 \right) \times 100. \quad (47)$$

Table 3 shows the value of PMSE in output simulation for different estimated models. The projection space model gives less PMSE in output, for estimation and with different validation datasets, than the other single-scale techniques. The small value of PMSE indicates good modeling performance and enhanced prediction ability of the proposed approach. The estimated model in projection space is able to capture all the system dynamics better due to the fact that it efficiently estimates the multiscale modes evolving at different timescale. On the other hand, single-scale techniques are able to estimate only an approximate model of the multiscale process thereby giving larger PMSE.

4.2. Case study using plant dataset

This subsection presents model estimation/validation exercise on transient dataset obtained from 540 MWe Indian pressurized heavy water reactor. The plant dataset includes reactor power as output and water level in zonal control compartment (ZCC) as input. The inflow variations in ZCC water level cause reactivity variations which result in changes in reactor power. Figs. 8 and 9, respectively, show variation in reactivity due to change in water level in ZCC and the corresponding variation in power.

Wavelet operators are designed as described in Subsections 3.2 and 3.3; this leads to the design of full PRBWFBs. The PRBWFBs are designed to have length of six taps and two vanishing moments as given in Table 4. The original measurement space system states are transformed by these operators to those in the projection space, and model parameters are estimated. System dynamics matrix of estimated projection space model is given by A_{j+1}^w

Table 2
Estimated wavelet filter coefficients for different states.

State	Estimated filters
First	$h[k] = [0, -0.35327, 0.49097, 0.75035, -1.24226, -1.00652, 0.14061, -0.00122]$
	$g[k] = [0, 0.56456, -0.78461, 0.25390, -0.03415, 0.00029, 0, 0]$
	$\bar{h}[k] = [0, 0, -0.00029, -0.03415, -0.25390, -0.78461, -0.56456, 0]$
	$\bar{g}[k] = [-0.00122, -0.14061, -1.00652, 1.24226, 0.75035, -0.49097, -0.35327, 0]$
Second	$h[k] = [0, 0.35326, -0.49089, -0.75038, 1.24207, 1.0066, -0.14046, 0.00121]$
	$g[k] = [0, -0.56462, 0.78461, -0.25380, 0.03410, -0.00029, 0, 0]$
	$\bar{h}[k] = [0, 0, 0.00029, 0.034106, 0.25380, 0.78461, 0.56462, 0]$
	$\bar{g}[k] = [0.00121, 0.14046, 1.00662, -1.24207, -0.75038, 0.49089, 0.35326, 0]$
Third	$h[k] = [0, -0.35324, 0.49081, 0.75041, -1.24187, -1.00671, 0.14030, -0.00120]$
	$g[k] = [0, 0.56468, -0.78460, 0.25369, -0.03405, 0.00029, 0, 0]$
	$\bar{h}[k] = [0, 0, -0.00029, -0.03405, -0.25369, -0.78460, -0.56468, 0]$
	$\bar{g}[k] = [-0.00120, -0.14030, -1.00671, 1.24187, 0.75041, -0.49081, -0.35324, 0]$
Fourth	$h[k] = [0, 0.35322, -0.49073, -0.75044, 1.24167, 1.00681, -0.14014, 0.00119]$
	$g[k] = [0, -0.56474, 0.78460, -0.25357, 0.03400, -0.00029, 0, 0]$
	$\bar{h}[k] = [0, 0, 0.00029, 0.03400, 0.25357, 0.78460, 0.56474, 0]$
	$\bar{g}[k] = [0.00119, 0.14014, 1.00681, -1.24167, -0.75044, 0.49073, 0.35322, 0]$
Fifth	$h[k] = [0, -0.35320, 0.49065, 0.75047, -1.24146, -1.00691, 0.13998, -0.00118]$
	$g[k] = [0, 0.56480, -0.78459, 0.25345, -0.03395, 0.00028, 0, 0]$
	$\bar{h}[k] = [0, 0, -0.00028, -0.03395, -0.25345, -0.78459, -0.56480, 0]$
	$\bar{g}[k] = [-0.00118, -0.13998, -1.00691, 1.24146, 0.75047, -0.49065, -0.35320, 0]$
Sixth	$h[k] = [0, 0.35318, -0.49056, -0.75051, 1.24124, 1.00702, -0.13980, 0.00117]$
	$g[k] = [0, -0.56487, 0.78459, -0.25333, 0.03390, -0.00028, 0, 0]$
	$\bar{h}[k] = [0, 0, 0.00028, 0.03390, 0.25333, 0.78459, 0.56487, 0]$
	$\bar{g}[k] = [0.00117, 0.13980, 1.00702, -1.24124, -0.75051, 0.49056, 0.35318, 0]$
Seventh	$h[k] = [0, -0.35316, 0.49047, 0.75054, -1.24103, -1.00713, 0.13963, -0.00116]$
	$g[k] = [0, 0.56494, -0.78458, 0.25321, -0.03384, 0.00028, 0, 0]$
	$\bar{h}[k] = [0, 0, -0.00028, -0.03384, -0.25321, -0.78458, -0.56494, 0]$
	$\bar{g}[k] = [-0.00116, -0.13963, -1.00713, 1.24103, 0.75054, -0.49047, -0.35316, 0]$

$$A^w_{j+1} = diag[\,0.0566, \quad 0.1107, \quad 0.9993\,]. \tag{48}$$

The estimation of neutron power by projection space model is shown in Fig. 9, which also compares estimates of power obtained by other empirical models. It may be seen that the projection space model suitably predicts the multiscale behavior and gives a better estimate of neutron power than do the other models. In case of ARX approach, the model structure estimates a noise model; however, the parameter of noise model is related to process model and thus

gives a poor estimate. Besides this, the OE model structure does not evaluate a noise model and approximates the noisy plant output as the output of the model. In SID, system parameters estimate Kalman states, which leads to a good response. Different estimated models are given in Appendix C.

For the purpose of validation of different estimated models, plant datasets are shown in Figs. 10 and 11. These plant datasets are comprised of data on changes in reactivity and corresponding variation in power. Outputs of all estimated models are compared with observed plant output in Fig. 11. It can be seen that single-scale
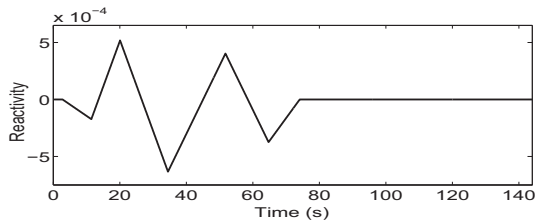

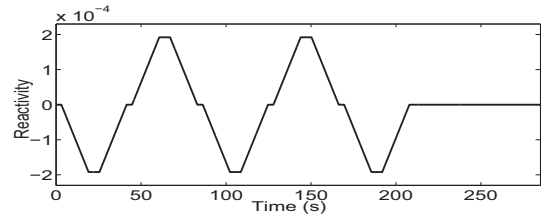**Fig. 4.** Variation of reference reactivity validation input (Case A).

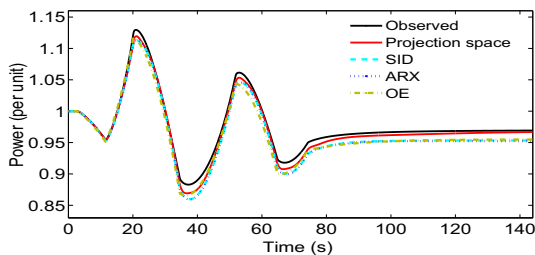**Fig. 6.** Variation of reference reactivity validation input (Case B).

Fig. 5. Outputs of estimated models with observed data for Case A input. ARX, Auto-Regressive with Exogenous input; OE, output error.
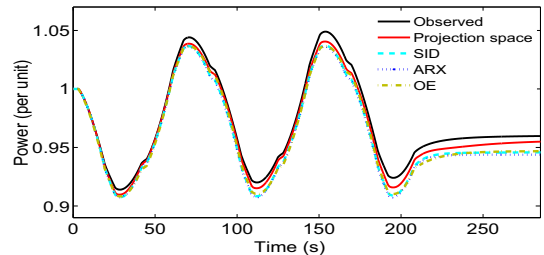

Fig. 7. Outputs of estimated models with observed data for Case B input. ARX, Auto-Regressive with Exogenous input; OE, output error.

Table 3
PMSE for simulated reference dataset.

Dataset	Model			
	Projection space	SID	ARX	OE
Estimation	2.3806×10^{-5}	5.0433×10^{-4}	7.9436×10^{-4}	3.6788×10^{-4}
Validation (Case A)	4.3000×10^{-3}	1.2000×10^{-2}	1.2900×10^{-2}	1.2500×10^{-2}
Validation (Case B)	2.8000×10^{-3}	1.0500×10^{-2}	1.2700×10^{-2}	1.0000×10^{-2}

ARX, Auto-Regressive with Exogenous input; OE, output error; PMSE, percentage mean squared error.
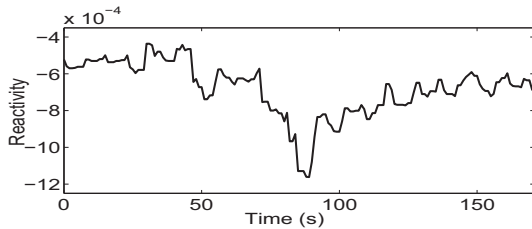

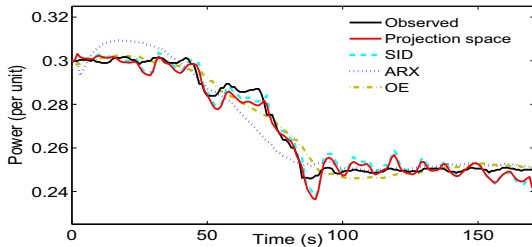**Fig. 8.** Variation of plant reactivity estimation input.

Fig. 9. Outputs of estimated models with observed data for plant input.
ARX, Auto-Regressive with Exogenous input; OE, output error.

Table 4
Estimated filter coefficients for different states for simulated plant dataset.

| State	Estimated filters
First	$h[k] = [-0.00497, 0.78317, 1.31746, 0.26550, -0.26381, 0]$
	$g[k] = [0, 0, 0.00303, -0.47679, 0.47376, 0]$
	$\bar{h}[k] = [0, 0.47376, 0.47679, 0.00303, 0, 0]$
	$\bar{g}[k] = [0, 0.26381, 0.26550, -1.31746, 0.78317, 0.00497]$
Second	$h[k] = [0.00477, -0.52473, -0.88623, -0.17917, 0.17754, 0]$
	$g[k] = [0, 0, -0.00645, 0.71031, -0.70385, 0]$
	$\bar{h}[k] = [0, -0.70385, -0.71031, -0.00645, 0, 0]$
	$\bar{g}[k] = [0, -0.17754, -0.17917, 0.88623, -0.52473, -0.00477]$
Third	$h[k] = [-0.02846, 0.49605, 0.89684, 0.19166, -0.18066, 0]$
	$g[k] = [0, 0, 0.04172, -0.72704, 0.68532, 0]$
	$\bar{h}[k] = [0, 0.68532, 0.72704, 0.04172, 0, 0]$
	$\bar{g}[k] = [0, 0.18066, 0.19166, -0.89684, 0.49605, 0.02846]$
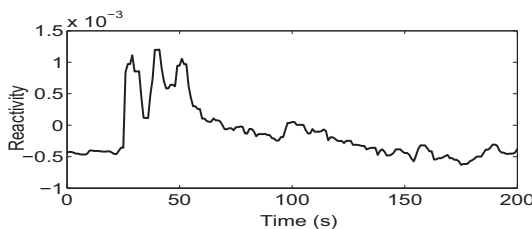
Fig. 10. Variation of plant reactivity validation input.
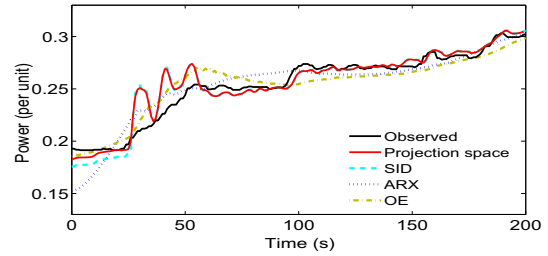

Fig. 11. Outputs of estimated models with observed data for plant input.
ARX, Auto-Regressive with Exogenous input; OE, output error.

Table 5
PMSE for simulated plant dataset.

Dataset	Model			
	Projection space	SID	ARX	OE
Estimation	1.2397×10^{-3}	1.3753×10^{-3}	3.5821×10^{-3}	1.4072×10^{-3}
Validation	1.1005×10^{-2}	1.2790×10^{-2}	1.3936×10^{-2}	1.2841×10^{-2}

ARX, Auto-Regressive with Exogenous input; OE, output error; PMSE, percentage mean squared error.

techniques are only able to approximate the multiscale process, whereas the estimated model in projection space efficiently captures system modes evolving at different scale of time, thus giving better prediction result than others. Table 5 shows the value of PMSE for different models for the estimation and validation datasets. It may be noted that the projection space approach yields less PMSE than do other single-scale techniques thereby outperforming other techniques in estimation and in validation in terms of mean squared error in the output.

5. Conclusion

One of the major achievements of this work is the formalization of a wavelet operator to transform states of a multivariable system from space of temporal measurements to that of projections in multiresolution, given by the operator. The imposed structure in projection space is justified as wavelets are approximate Eigen functions of convolution operators. It is also shown that given an operator, there exists a definite relationship between the model in the measurement space and that in the projection space. The design methodology is demonstrated by designing multirate filter bank associated with wavelet operators for modeling a nuclear reactor. A nuclear reactor is an ideal example to establish the methodology as it exhibits multi-timescale complex behavior. Furthermore, it is shown that projection space modeling of the reactor system leads to significant improvement in output prediction over single-scale modeling techniques.

Conflicts of interest

There is no conflict of interest.

Appendix A

Vandermonde structure of $\mathscr{W}_j$

General structure of the linear transformation $\mathscr{W}_j$ satisfying $A_{j+1}^w \mathscr{W}_j = \mathscr{W}_j \tilde{A}$ is computed as follows.

Let

$$
\mathscr{W}_j = \begin{bmatrix} v_{11} & v_{12} & \cdots & v_{1N} \\ v_{21} & v_{22} & \cdots & v_{2N} \\ \vdots & \vdots & \ddots & \vdots \\ v_{N1} & v_{N2} & \cdots & v_{NN} \end{bmatrix}. \tag{A.1}
$$

Then,

$$
\begin{bmatrix} \alpha_1 & 0 & \cdots & 0 \\ 0 & \alpha_2 & \cdots & 0 \\ \vdots & \vdots & \ddots & \vdots \\ 0 & 0 & \cdots & \alpha_N \end{bmatrix} \begin{bmatrix} v_{11} & v_{12} & \cdots & v_{1N} \\ v_{21} & v_{22} & \cdots & v_{2N} \\ \vdots & \vdots & \ddots & \vdots \\ v_{N1} & v_{N2} & \cdots & v_{NN} \end{bmatrix}
$$
$$
= \begin{bmatrix} v_{11} & v_{12} & \cdots & v_{1N} \\ v_{21} & v_{22} & \cdots & v_{2N} \\ \vdots & \vdots & \ddots & \vdots \\ v_{N1} & v_{N2} & \cdots & v_{NN} \end{bmatrix} \begin{bmatrix} 0 & 0 & \cdots & -a_N \\ 1 & 0 & \cdots & -a_{N-1} \\ 0 & 1 & \cdots & -a_{N-2} \\ \vdots & \vdots & \ddots & \vdots \\ 0 & 0 & \cdots & -a_1 \end{bmatrix} \tag{A.2}
$$

implies

$$
\begin{aligned}
\alpha_i v_{i1} &= v_{i2}, \\
\alpha_i v_{i2} &= v_{i3}, \\
&\vdots \\
\alpha_i v_{i(N-1)} &= v_{iN}, \\
\alpha_i v_{iN} &= -a_N v_{i1} - a_{N-1} v_{i2} \cdots - a_1 v_{iN}, \forall i = 1, 2, ..., N.
\end{aligned} \tag{A.3}
$$

Because α_i, $i = 1, 2, ..., N$ are the eigenvalues of $\overline{A}_j^v$, one can write

$$
\begin{aligned}
v_{iN} &= \alpha_i v_{1(N-1)} = \alpha_i^2 v_{i(N-2)} = \cdots = \alpha_i^{(N-1)} v_{i1}, \\
v_{i(N-1)} &= \alpha_i v_{1(N-2)} = \alpha_i^2 v_{i(N-3)} = \cdots = \alpha_i^{(N-2)} v_{i1}, \\
&\vdots \\
v_{i2} &= \alpha_i v_{i1}, \\
&\forall i = 1, 2, ..., N.
\end{aligned} \tag{A.4}
$$

One can assume $v_{i1} = m_i$, $\forall\ i = 1, 2, ..., N$ to get the *Vandermonde* structure of $\mathscr{W}_j$ as given in (30).

Appendix B

An analytical example of PRBWFB design

Consider that the analysis HPF coefficients g are known to us as

$$
g = [g_1 \quad g_2 \quad g_3 \quad g_4]. \tag{B.1}
$$

Using perfect reconstruction condition, synthesis LPF coefficients $\tilde{h}$ are given by

$$
\tilde{h} = [-g_4 \quad g_3 \quad -g_2 \quad g_1]. \tag{B.2}
$$

Let the analysis LPF h, to be computed, is given by

$$
h = [h_1 \quad h_2 \quad h_3 \quad h_4]. \tag{B.3}
$$

Applying the biorthogonality condition between h and g,

$$
\begin{aligned}
-h_1 g_4 + h_2 g_3 - h_3 g_2 + h_4 g_1 &= 1, \\
-h_1 g_2 + h_2 g_1 &= 0, \\
-h_3 g_4 + h_4 g_4 &= 0.
\end{aligned} \tag{B.4}
$$

To design the filter bank with one vanishing moment constrain, the vanishing moment condition is given by

$$
-h_1 + h_2 - h_3 + h_4 = 0. \tag{B.5}
$$

The system of Equations (B.4) and (B.5) give coefficients of analysis LPF h, and further synthesis HPF $\tilde{g}$ is designed.

$$
\tilde{g} = [h_4 \quad -h_3 \quad h_2 \quad -h_1]. \tag{B.6}
$$

Similarly, the design can be extended for desired number of vanishing moments after increasing length of filter by appending zeros to it.

Appendix C

Basic Model Structures

The general parametric discrete-time model structure is given by [29].

$$
y[k] = \frac{B(q^{-1})}{A(q^{-1})} u[k] + \frac{C(q^{-1})}{D(q^{-1})} e[k], \tag{C.1}
$$

where q^{-1} is backward shift operator such that $q^{-1}u[k] = u[k-1]$. The polynomials are defined as

$$
\begin{aligned}
B(q^{-1}) &= b_1 q^{-1} + b_2 q^{-2} + \cdots + b_{n_b} q^{-n_b}, \\
A(q^{-1}) &= 1 + a_1 q^{-1} + a_2 q^{-2} + \cdots + a_{n_a} q^{-n_a}, \\
C(q^{-1}) &= 1 + c_1 q^{-1} + c_2 q^{-2} + \cdots + c_{n_c} q^{-n_c}, \\
D(q^{-1}) &= 1 + d_1 q^{-1} + d_2 q^{-2} + \cdots + d_{n_d} q^{-n_d}.
\end{aligned} \tag{C.2}
$$

The OE model structure is defined by choosing $D(q^{-1}) = C(q^{-1}) = 1$ in (C.1). It is given by

$$
y[k] = \frac{B(q^{-1})}{A(q^{-1})} u[k] + e[k]. \tag{C.3}
$$

The parameters of estimated OE model from reference dataset are given by

$$
\begin{aligned}
B(q^{-1}) &= 186.9 q^{-1} - 370.9 q^{-2} + 184 q^{-3}, \\
A(q^{-1}) &= 1 - 1.994 q^{-1} + 0.994 q^{-2}.
\end{aligned} \tag{C.4}
$$

The ARX model structure is defined by choosing $C(q^{-1})=1$ and $D(q^{-1})=A(q^{-1})$ in (C.1). It is given by

$$
y[k] = \frac{1}{A(q^{-1})} \left(B(q^{-1}) u[k] + e[k] \right). \tag{C.5}
$$

The parameters of estimated ARX model from reference dataset are given by

$$
\begin{aligned}
B(q^{-1}) &= 61.47 q^{-1} - 121 q^{-2} + 59.58 q^{-3}, \\
A(q^{-1}) &= 1 - 2.582 q^{-1} + 2.168 q^{-2} - 0.586 q^{-3},
\end{aligned} \tag{C.6}
$$

and the estimated SID model from reference data is given by

$$
\begin{aligned}
x[k+1] &= \begin{bmatrix} 1 & 0 & 0 \\ -0.001 & 0.891 & -0.120 \\ -0.004 & -0.238 & 0.693 \end{bmatrix} x[k] + \begin{bmatrix} 1.5 \\ 28082 \\ 68668 \end{bmatrix} u[k] \\
&\quad + \begin{bmatrix} 0.022 \\ -997 \\ 2860 \end{bmatrix} e[k], \\
y[k] &= [53.69 \quad -0.0007 \quad 0] x[k] + e[k].
\end{aligned} \tag{C.7}
$$

On the other hand, estimated models from plant dataset are as follows:The OE model is given by

$$B\left(q^{-1}\right) = -3.83q^{-1} + 31.55q^{-2} - 28.27q^{-3},$$
$$A\left(q^{-1}\right) = 1 - 1.042q^{-1} - 0.841q^{-2} + 0.883q^{-3}. \tag{C.8}$$

The ARX model is given by

$$B\left(q^{-1}\right) = -15.63q^{-1} + 42.93q^{-2} - 25.92q^{-3} - 41.9q^{-4}$$
$$+ 66.34q^{-5} - 25.92q^{-6},$$
$$A\left(q^{-1}\right) = 1 - 2.867q^{-1} + 2.789q^{-2} - 0.975q^{-3} + 0.0541q^{-4}, \tag{C.9}$$

and the SID model is given by

$$x[k+1] = \begin{bmatrix} 0.999 & -0.003 & 0.004 \\ 0.083 & 0.454 & 0.272 \\ 0.122 & -0.828 & -0.509 \end{bmatrix} x[k] + \begin{bmatrix} 19.035 \\ 2364.8 \\ 94.335 \end{bmatrix} u[k]$$
$$+ \begin{bmatrix} 0.125 \\ 2.266 \\ 0.152 \end{bmatrix} e[k],$$

$$y[k] = \begin{bmatrix} 7.703 & -0.001 & 0.003 \end{bmatrix} x[k] + e[k]. \tag{C.10}$$

References

[1] P.V. Kokotovic, R.E. O'Malley, P. Sannuti, Singular perturbations and order reduction in control theory: an overview, Automatica 12 (1976) 123–132.

[2] R.G. Phillips, Reduced order modeling and control of two-time-scale discrete systems, Int. J. Control 31 (1980) 765–780.

[3] D.S. Naidu, Singular perturbations and time scales in control theory and applications, Dyn. Contin. Discret. Impuls Sys. Ser. B: Appl. Algorithms 9 (2002) 233–278.

[4] S.R. Shimjith, A.P. Tiwari, B. Bandyopadhyay, A three-timescale approach for design of linear state regulator for spatial control of advanced heavy water reactor, IEEE Trans. Nuclear Sci. 58 (3) (2011) 1264–1276.

[5] M. Boroushaki, M.B. Ghofrani, C. Lucas, M.J. Yazdanpanah, Identification and control of a nuclear reactor core (VVER) using recurrent neural networks and fuzzy systems, IEEE Trans. Nuclear Sci. 50 (1) (Feb 2003) 159–174.

[6] C. Shiguo, Z. Ruanyu, W. Peng, L. Taihua, Enhance accuracy in pole identification of system by wavelet transform de-noising, IEEE Trans. Nuclear Sci. 51 (1) (Feb. 2004) 250–255.

[7] F. Previdi, S.M. Savaresi, P. Guazzoni, L. Zetta, Detection and clustering of light charged particles via system-identification techniques, Int. J. Adapt. Control Signal Process. 21 (2007) 375–390.

[8] S.G. Mallat, A theory for multiresolution signal decomposition: the wavelet representation, IEEE Trans. Pattern Anal. Machine Intell. 11 (7) (1989) 674–693.

[9] K.C. Chou, A.S. Willsky, A. Benveniste, Multiscale recursive estimation, data fusion, and regularization, IEEE Trans. Autom. Control 39 (3) (1994) 464–478.

[10] D. Coca, S.A. Billings, Non-linear system identification using wavelet multi-resolution models, Int. J. Control 74 (18) (2001) 1718–1736.

[11] X.W. Chang, L. Qu, Wavelet estimation of partially linear models, Comput. Stat. Data Anal. 47 (1) (2004) 31–38.

[12] N.V. Troung, L. Wang, P.C. Young, Non-linear system modelling based on non-parametric identification and linear wavelet estimation of SDP models, In. J. Control 80 (5) (2007) 774–788.

[13] Y. Li, H.L. Wei, S.A. Billings, Identification of time-varying systems using multi-wavelet basis functions, IEEE Trans. Control Sys. Technol. 19 (3) (2011) 656–663.

[14] F. He, H.L. Wei, S.A. Billings, Identification and frequency domain analysis of non-stationary and nonlinear systems using time-varying NARMAX models, Int. J. Sys. Sci. 46 (11) (2015) 2087–2100.

[15] G. Heo, S.S. Choi, S.H. Chang, Thermal power estimation by fouling phenomena compensation using wavelet and principal component analysis, Nuclear Eng. Design 199 (2000) 31–40.

[16] G.Y. Park, J. Park, P.Y. Seong, Application of wavelets noise-reduction technique to water-level controller, Nuclear Technol. 145 (2004) 177–188.

[17] V. Vajpayee, S. Mukhopadhyay, A.P. Tiwari, Subspace-based wavelet preprocessed data-driven predictive control, INCOSE Int. Symp. 26 (s1) (2016) 357–371.

[18] G. Espinosa-Paredes, A. Nunez-Carrera, A. Prieto-Guerrero, M. Cecenas, Wavelet approach for analysis of neutronic power using data of ringhals stability benchmark, Nuclear Eng. Design 237 (2007) 1009–1015.

[19] A. Prieto-Guerrero, G. Espinosa-Paredes, Decay ratio estimation of bwr signals based on wavelet ridges, Nuclear Sci. Eng. 160 (3) (2008) 302–317.

[20] M. Antonopoulos-Domis, T. Tambouratzis, System identification during a transient via wavelet multiresolution analysis followed by spectral techniques, Ann. Nuclear Energy 25 (6) (1998) 465–480.

[21] T. Tambouratzis, M. Antonopoulos-Domis, Parameter estimation during a transient application to BWR stability, Ann. Nuclear Energy 31 (18) (2004) 2077–2092.

[22] S. Mukhopadhyay, A.P. Tiwari, Consistent output estimate with wavelets: an alternative solution of least squares minimization problem for identification of the LZC system of a large PHWR, Ann. Nuclear Energy 37 (2010) 974–984.

[23] V. Vajpayee, S. Mukhopadhyay, A.P. Tiwari, Multiscale subspace identification of nuclear reactor using wavelet basis function, Ann. Nuclear Energy 111 (2018) 280–292.

[24] A. Gabor, C. Fazekas, G. Szederkenyi, K.M. Hangos, Modeling and identification of a nuclear reactor with temperature effects and xenon poisoning, Eur. J. Control 17 (1) (2011) 104–115.

[25] L. Hong, G. Cheng, C.K. Chui, A filter-bank-based kalman filtering technique for wavelet estimation and decomposition of random signals, IEEE Trans. Circuits Sys. II: Analog Digit. Signal Process. 45 (2) (1998) 237–241.

[26] H.M. Nounou, M.N. Nounou, Multiscale fuzzy kalman filtering, Eng. Appl. Artif. Intell. 19 (5) (2006) 439–450.

[27] E.G. Gilbert, Controllability and observability in multivariable control systems, J. SIAM Control 1 (2) (1963) 128–151.

[28] B. Friedland, Control Systems Design: an Introduction to State-space Methods, McGraw-Hill Higher Education, 1985.

[29] L. Ljung, System Identification: Theory for the User, second ed., Prentice Hall, Upper Saddle River, NJ, 1999.